J Mar Sci Technol (2009) 14:296–309
DOI 10.1007/s00773-009-0043-8

ORIGINAL ARTICLE

A proposal for propulsion performance prediction of a single-propeller twin-rudder ship

Vishwanath Nagarajan · Dong-Hoon Kang · Kazuhiko Hasegawa · Kenjiro Nabeshima · Toshihiko Arii

Received: 31 January 2008 / Accepted: 3 January 2009 / Published online: 5 March 2009

Abstract The influence of a rudder's axial force on the prediction of full-scale powering performance of a ship is investigated in this paper. Axial force characteristics of different rudder types were investigated by open water experiments. Viscous scale effects on the rudder's axial force were investigated by carrying out open water experiments with different sizes of rudder. Experiments were carried out in the towing tank for a model ship fitted with different rudder systems to investigate the influence of rudder's axial force on full-scale propulsion performance prediction. Based on the experiment results, a new prediction method is proposed for estimating full-scale power that considers scale effect on rudder's axial force. Good performance of the proposed prediction method is demonstrated by estimating the engine power of a ship installed with a special high lift twin-rudder system from model experiments and comparing it with the values measured on the ship during full-scale experiments.

Keywords Single-propeller twin-rudder system · Rudder axial force · Viscous scale effects

V. Nagarajan (✉) · K. Hasegawa
Department of Naval Architecture and Ocean Engineering, Graduate School of Engineering, Osaka University, 2-1 Yamadaoka, Suita 565-0871, Japan
e-mail: Vishwanath@naoe.eng.osaka-u.ac.jp

D.-H. Kang
100 C. Maxwell Stanley Hydraulics Laboratory, IIHR-Hydroscience and Engineering, College of Engineering, The University of Iowa, Iowa City, IA 52242-1585, USA

K. Nabeshima · T. Arii
Japan Hamworthy Co., Ltd, Omodaka Building, 1-15-1 Shigino-nishi, Joto-ku, Osaka 536-0014, Japan

List of symbols

A_L	Longitudinal projected area of ship above waterline
A_T	Transverse projected area of ship above waterline
B	Ship's breadth
B_R	Distance between the center of rudderstock of the port and starboard twin rudder
C_B	Block coefficient
C_F	Frictional resistance coefficient of ship as per ITTC formula
$C_{FR\{S\}_P}$	Frictional resistance coefficient of a twin rudder
C_R	Rudder chord
$C_{SR\{S\}_P}$	Pressure drag due to flow separation of a twin rudder
d_A	Ship's draft at aft perpendicular
d_F	Ship's draft at forward perpendicular
D_P	Propeller diameter
F_N, $F_{N\{S\}_P}$	Normal force for a single and twin rudder, respectively
F_X, $F_{X\{S\}_P}$	Axial force for a single and twin rudder, respectively
H	Rudder height
J	Propeller advance coefficient
K	Form factor for ship
K_Q	Propeller open water torque coefficient
$K_{R\{S\}_P}$	Form factor for a twin rudder
K_T	Propeller open water thrust coefficient
L	Ship's length between perpendiculars
L_{OA}	Ship's length overall
LCG	Ship's longitudinal center of gravity
n	Propeller revolution
N	Yawing moment acting on the ship
P	Propeller pitch

Q	Propeller torque
r	Ship's yaw rate
Rn	Reynolds number
R_T	Total resistance of ship
S_{BK}	Wetted surface area of bilge keel
S_R, $S_{R\{S\}_{\{P\}}}$	Projected rudder area based on chord for a single and twin rudder, respectively
S_W	Wetted surface area of ship excluding rudder and bilge keel
SFC	Skin friction correction
T	Propeller thrust
t_{P0}	Thrust deduction fraction for propeller at ship's zero drift angle
t_R	Coefficient for reduction of rudder's resistance in ship's surge direction
u	Surge velocity at ship's center of gravity
u_p	Inflow velocity in longitudinal direction to propeller
u_R, $u_{R\{S\}_{\{P\}}}$	Inflow velocity in longitudinal direction to a single rudder and twin rudder
U	Total velocity at ship's center of gravity, $U = \sqrt{u^2 + v^2}$
U_W	Wind speed in earth coordinate.
v	Sway velocity at ship's center of gravity
w_{P0}	Wake fraction for propeller at ship's zero drift angle
w_R, $w_{R\{S\}_{\{P\}}}$	Wake fraction for single and twin rudder
X	Force on ship in surge direction
X_R	Force on ship due to rudder in surge direction
Y	Force on ship in sway direction
β	Ship's drift angle
δ, $\delta_{\{S\}_{\{P\}}}$	Angle of single and twin rudder
δ_0, $\delta_{\{S\}_{\{P\}}0}$	Angle at which normal lift force F_N, $F_{N\{S\}_{\{P\}}}$ is zero
ΔC_F	Hull roughness allowance
ε, $\varepsilon_{\{S\}_{\{P\}}}$	Ratio of wake fraction of rudder to propeller
η	Ratio of propeller diameter to rudder height
η_R	Relative rotative efficiency
κ, $\kappa_{\{S\}_{\{P\}}}$	Propeller race amplification factor for a single and a twin rudder, respectively
ρ	Density of water (model scale, fresh water; full-scale, sea water)
ψ	Ship's heading angle
ψ_W	Direction of wind in earth coordinates

Subscript

S Starboard twin rudder
P Port twin rudder

1 Introduction

The number of ships constructed every year is growing quickly due to a corresponding rise in the shipping trade. With petroleum energy reserves falling and waterways becoming more crowded, there is a simultaneous push for maximizing cargo carrying capacity, improving the fuel efficiency and increasing the maneuverability of ships. Main engine manufacturers are continually reducing engine revolution to maximize fuel efficiency. This has resulted in a corresponding increase in propeller diameter to maintain the required thrust and speed at lower propeller revolutions. To accommodate a larger diameter propeller, the designs of stern hull forms have also undergone several changes. The stern hull form with a rudder shoe piece, which was a common design for smaller diameter propeller, has been replaced by the stern bulb design. The stern bulb design has an extended rudder horn and extra pintles to bear the rudder loads released by the shoe piece. However, earlier ships, especially very large crude carriers (VLCC), with this design were found to track a course poorly, and several studies concluded that the stern bulb hull form requires a larger area for mariner-type rudder with NACA section than the earlier design. Yamada [1] has given an overview of these developments. The maneuvering aspects of such vessels are still being studied and various means are being explored to improve them.

For a mariner-type rudder with NACA cross-section, it is recommended that configurations like two rudders with a single propeller be avoided [2]. However, a design with a single-propeller twin-rudder system, Vectwin rudder [3], with a unique rudder cross-section, was successfully introduced for small vessels for improving their maneuverability. A variant of this design has been introduced for improving the maneuverability of large ships up to the size of a VLCC [4]. There are some other advantages of this type of rudder system. In high speed ships, since the twin rudder is not directly in the propeller race, erosion of the rudder surface due to propeller hub vortex or cavitations may be avoided [5]. Moreover, as the twin rudder is compact, a ship's cargo carrying capacity can be increased within existing ship dimensions. Suitability of single-propeller twin-rudder system for large vessels like VLCCs was confirmed by Hasegawa et al. [6]. They concluded that the single-propeller twin-rudder system is suitable for maneuvering a VLCC and also showed that with a suitable combination of rudder angle and propeller revolution, the stopping distance of a VLCC can be lower by about 2–3 ship lengths than a single-propeller, single-rudder system. Kang et al. [7] developed a mathematical model of a single propeller twin-rudder ship, validated the model with free running experiments and made some recommendations for its installation.

However, no detailed study has been carried out on the full-scale propulsion performance prediction of ships fitted with special rudder systems like the Schilling rudder, a single-propeller twin-rudder system, etc. For propulsion performance prediction of ships from model experiments,

scale effect is important. A guideline for propulsion performance prediction of single screw ships from model experiments was developed by the International Towing Tank Conference (ITTC) [8]. The guideline is widely used for ships fitted with mariner rudders; however, it is known that it may not be suitable if some appendages like a rudder, pod unit, etc. that has significant axial force component is installed on the ship. Therefore, for ships having special propulsion systems, like a pod unit, some recommendation for scaling of viscous resistance has been devised [9]. However, no such guideline exists for scaling viscous resistance of special rudder systems like the Schilling rudder, a single propeller twin-rudder system, etc. It is reported that in the case of these special rudder systems, the predicted full-scale power from model experiments by ITTC [8] method is usually higher than the power measured during sea trials and actual operation.

In this paper, the axial force characteristics of different rudder systems are determined from experiments. The influence of these characteristics on a ship's full-scale powering prediction is investigated. A method of predicting full-scale power considering these characteristics is then proposed. The full-scale power is predicted from model experiments by either considering or ignoring the rudder's axial force characteristics. The predicted power is compared with power measured during full-scale experiments. It is shown that it is important to consider rudder's axial force characteristics, especially for ships fitted with special rudder systems like a single-propeller twin-rudder system.

2 Description of the procedure

In this paper, a single-propeller, single-rudder system is referred to as a single-rudder system and a single-propeller twin-rudder system is referred as a twin-rudder system, respectively. One of the earliest works showing the influence of rudder type on the thrust deduction fraction estimated from model experiments was done by Todd [10]. He conducted self-propulsion experiments on a model ship with and without the rudder and associated appendages, and their influence on thrust deduction coefficient was shown. Experiments were conducted with different rudder sections to show the influence of the rudder type. Earlier, different experimental facilities had their own procedure regarding installing appendages like rudder, bilge keels, etc. on the model during experiments. For easy interpretation of experiment data, a standardized format for conducting model resistance and self-propulsion experiments was introduced by the ITTC. In the ITTC method, explicit correction for appendages like the bilge keel is mentioned, while it is implied that the rudder is installed during the experiments. Additionally, the viscous scale effects are considered for the ship as a whole, i.e. there is no scaling of viscous resistance for the appendages. If the rudder resistance component is high, the viscous scale effect on rudder resistance and their influence on full-scale propulsion performance prediction are expected to be significant. This is because the average flow speed over the rudder and the average flow speed over the ship are different and the length of the ship and the rudder are different; thus, the Reynolds number of the respective average flow speeds will be different.

To see the above influences, two different analysis methods are followed for single and twin-rudder systems, respectively. One is the well-known ITTC method, which is called the "conventional method". In the other method, the resistance of rudder and ship is considered separately, and it is called the "proposed method". The coordinate system shown in Fig. 1 is followed for analysis of a twin-rudder system. For a single-rudder system, in Fig. 1, the twin rudder is replaced by a single rudder and the subscripts 'P' and 'S' are not used in the rudder parameters.

2.1 Ship resistance

The resistance coefficient is defined as per the "conventional method". During the resistance experiments, the propeller is removed and the shaft end fitted with a fair water cap. For the "proposed method" during resistance experiments, rudder skeg is fitted, while the rudder is removed from the ship model. The form factor (K) is estimated from model experiment results [11] using three dimensional viscous resistance formulation.

2.2 Rudder resistance

For rudders with NACA section, axial force is shown to be a function of Reynolds number and angle of attack [12, 13].

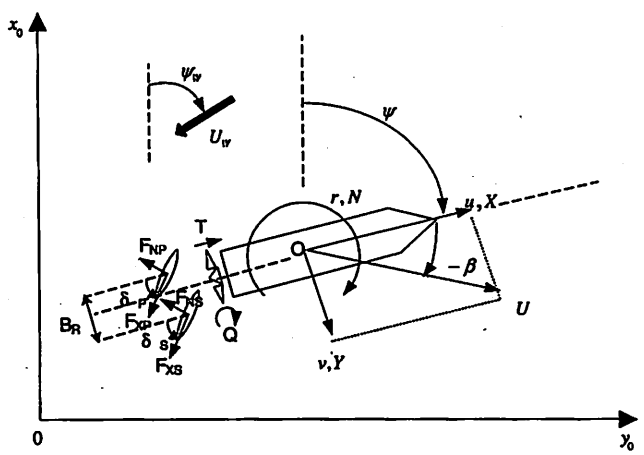

Fig. 1 Coordinate system

The single rudder used for subject model has modified NACA section, so its axial force coefficient is considered as Eq. 1

$$F_X/(0.5\rho 2S_R u_R^2) = f(Rn, \delta). \quad (1)$$

For special rudder systems like the twin-rudder, the axial force characteristic is different than in the single rudder. This is due to their different cross-section and due to the end plates fitted on the top and bottom of the rudder. For such rudder system, the axial force is considered to have two components, viscous resistance with form drag and pressure resistance due to flow separation as shown in Eq. 2

$$F_{X\{P\}}^{S}\Big/\left(0.5\rho S_{R\{P\}}^{S} u_{R\{P\}}^{2S}\right) = \left(1+K_{R\{P\}}^{S}\right)C_{FR\{P\}}^{S} + C_{SR\{P\}}^{S}. \quad (2)$$

In Eq. 2, the subscripts 'P' and 'S' in parenthesis '{}' refer to port and starboard twin-rudder, respectively. This method of writing the equations will be followed in this paper. When referring to single rudder, the subscripts 'P' and 'S' are not used as shown in Eq. 1.

2.3 Inflow into rudder

For the "proposed method", the inflow into rudder needs to be modeled. The MMG model for rudder inflow velocity is modified for the twin-rudder system as shown in Eq. 3

$$u_{R\{P\}}^{S} = \varepsilon_{\{P\}}^{S} u_P \sqrt{\eta\left[1+\kappa_{\{P\}}^{S}\left(\sqrt{1+\frac{8K_T}{\pi J^2}}-1\right)\right]^2+(1-\eta)} \quad (3)$$

where $\varepsilon_{\{P\}}^{S} = \frac{1-w_{R\{P\}}^{S}}{1-w_{P0}}$, $\eta = \frac{D_P}{H}$, $u_p = (1-w_{P0})u$.

2.4 Hull rudder interaction coefficients

In the MMG model for the single rudder, the component of rudder's normal lift force in ship's surge direction is expressed as Eq. 4 [14, 15], while the rudder's axial force component in ship's surge direction is assumed included in ship's resistance.

$$X_R = -(1-t_R)(F_N \sin\delta) \quad (4)$$

In the "proposed method", the rudder is not fitted on the model during resistance experiments. Therefore, to include rudder's axial force in ship's surge direction, Eq. 4 is rewritten as Eq. 5

$$X_R = -(1-t_R)(F_{XS}\cos\delta_S + F_{NS}\sin\delta_S + F_{XP}\cos\delta_P + F_{NP}\sin\delta_P). \quad (5)$$

2.5 Hull propeller interactions

The method of estimating the coefficient t_{P0} by the "conventional method" is shown in Eq. 6

$$1-t_{P0} = \frac{(R_T)_{\text{Hull+rudder}} - (\text{SFC})_{\text{Hull+rudder}}}{(T)_{\text{Hull+rudder}}}. \quad (6)$$

For the "proposed method", since the rudder is not fitted on the model during resistance experiments, the method of estimating the coefficient t_{P0} is modified as shown in Eq. 7

$$1-t_{P0} = \frac{(R_T)_{\text{Hull}} - (\text{SFC})_{\text{Hull}} + (X_R)_{\text{Rudder behind propeller}}}{(T)_{\text{Hull+Rudder}}}. \quad (7)$$

For estimating coefficients w_{P0} and η_R, the model ship's resistance data is not used and since the rudder is fitted during self-propulsion experiments, the influence of the hull and rudder is included in these coefficients. Therefore, w_{P0} and η_R for the "proposed method" are determined using the "conventional method" as shown in Eq. 8

$$\left.\begin{aligned} K_T &= \frac{(T)_{\text{Hull+rudder}}}{\rho n^2 D_P^4} \\ 1-w_{P0} &= \frac{JD_P n}{U} \\ \eta_R &= \frac{(Q)_{\text{Hull+rudder}}}{(Q)_{\text{Open water}}} \end{aligned}\right\}. \quad (8)$$

Coefficient w_{P0} determined for the model ship is scaled to full ship using "conventional method" as shown in Eq. 9

$$(w_{P0})_{\text{Ship}} = (t_{P0}+\phi) + \left((w_{P0})_{\text{Model}} - t_{P0} - \phi\right) \times \frac{(1+K)(C_F)_{\text{Ship}} + \Delta C_F}{(1+K)(C_F)_{\text{Model}}} \frac{(S_W + 2S_R + S_{BK})}{(S_W + 2S_R)}. \quad (9)$$

The coefficient ϕ in Eq. 9, represents the influence of the rudder on the wake fraction in way of propeller, when the rudder is fitted behind the propeller. The recommended value of ϕ is 0.04 [8] for a single-rudder system. The value of ϕ needs to be investigated for a twin rudder due to their different geometric layout.

3 Validation of the procedure by experiments

3.1 Experiment facility and procedure

The open water experiments for rudder were carried out in the circulating water tank of Osaka University. The open water experiments for the propeller, model ship resistance and self-propulsion experiments were carried out in the towing tank of Osaka University. The full-scale experiment was carried out in Saeki Bay, in Japan's Seto Inland Sea.

The speed and engine power during the full-scale experiments were measured and provided by the shipyard.

The measurement section of the circulating water channel is 2.0 m long, 0.9 m wide and 0.5 m deep. The maximum flow speed attainable in the measurement section is 1.2 m/s. The details of the towing tank are available at the website http://www.naoe.eng.osaka-u.ac.jp/eng/info_course/equip.html. A DC motor rotates the propeller and each rudder is turned using a five phase stepping motor. The propeller revolution and rudder angle are controlled through computer.

During resistance and self-propulsion experiments, for measuring the forces and moment on the rudder, the ship and the propeller (thrust and torque) strain gauge-type transducers were used. During propeller open water experiments, for measuring the thrust and torque, duplex-balance rod-deflection-type dynamometer was used. Signals from the transducers are electronically filtered and amplified, and fed to the computer through a 12-bit analog—digital converter board. A sampling frequency of 100 Hz is used for all the experiments. The propeller revolution and towing carriage speed are directly fed to the computer through a digital input output board. During experiments, all the measurements are monitored on the computer screen. The resistance and self-propulsion tests are for model-free conditions (free to sink and trim) and were carried out using standard towing tank procedures. During experiment in towing tank, a time interval of about 15 min between carriage runs was maintained in order to damp the fluid motion induced by previous run.

3.2 Model ship

The principal particulars of the model ship are shown in Table 1. Model ship A was used for comparing the single-rudder and twin-rudder systems and for developing the new prediction method of full-scale power. Model ship B has a full-scale equivalent and was installed with a twin-rudder system. It was used for comparing the power predicted by model experiments with the values measured during full-scale experiments. Both model ships were fabricated from wood. Studs of 2.0 mm depth were nailed to the surface of the model ship at 10.0 mm pitch at SS $9\frac{1}{2}$ and at the midsection of the bulbous bow to stimulate turbulent flow. Model ship A has a bow thruster tunnel. During the experiments in the towing tank, the bow thruster tunnel was blanked using a streamlined cap and the ship surface in the way of the tunnel opening was made smooth by using water resistant tape. Neither of the model ships was fitted with a bilge keel. The stock propeller of the Osaka University was used for both model ships. The layout of the stern section of model ship A is shown in Fig. 2. Model ship A is fitted with a detachable type of stern that can be changed to suit both single-rudder and twin-rudder systems. Four types of rudders, single, twin (type I, type II and type III) were fabricated for the experiments. Model ship B was fitted with a twin-rudder system (type III) that was also installed on the full-scale ship. The particulars of the different rudder systems are shown in Table 2. Two different sizes of twin rudder (type III) were fabricated in the scale ratios 1:28.2 (type A) and 1:9.5 (type B), respectively. The twin-rudder (type III, B) system was fabricated exclusively for rudder open water experiments to investigate the scale effects on rudder resistance. The mariner rudder with a shallow horn and a modified NACA cross-section is well known. A brief description of twin-rudder system will be given. The layout of the twin-rudder system is shown in

Table 1 Principal particulars of model ship

Particulars	Model ship A	Model ship B
L (m)	3.94	3.52
B (m)	0.58	0.57
d_A (m)	0.22	0.25
d_F (m)	0.22	0.20
LCG/L	0.037	0.010
C_B	0.83	0.718
S_W (m^2)		
Single-rudder skeg	3.541	N/A
Twin-rudder skeg	3.558	2.927
Propeller		
D_P (m)	0.1206	
P (m)	0.08041	
Number of blades	5	

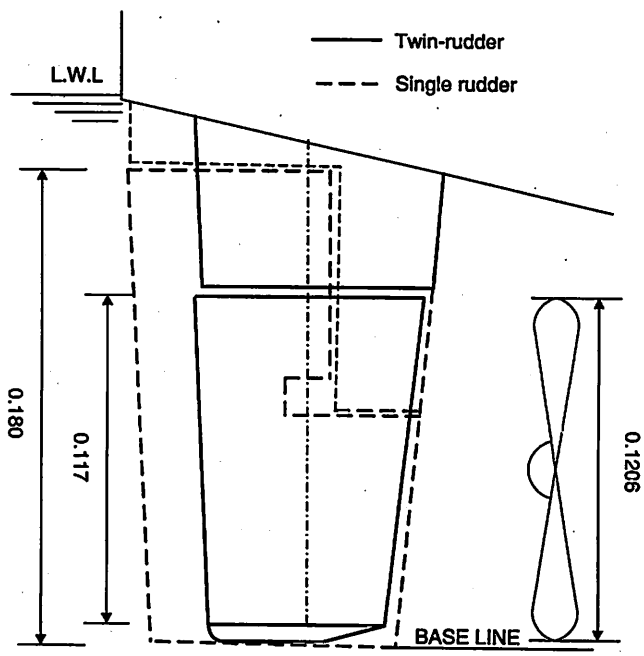

Fig. 2 Layout of a twin rudder and single rudder. Model ship A

Table 2 Particulars of different rudder systems

Coefficients	Single rudder (model ship A)	Twin rudder			
		Type I (model ship A)	Type II (model ship A)	Type III (model ship B)	
				Type A	Type B
H (m)	0.1800	0.1170	0.1190	0.1350	0.4000
C_R (m)	0.1070	0.0720	0.0740	0.0990	0.2950
S_R, $S_{R\{P\}}^{\{S\}}$ (for one rudder, m^2)	0.0158	0.0084	0.0088	0.0134	0.1190
B_R (m)	0.0000	0.0648	0.0648	0.0830	0.7371

The area is determined from chord and is not wetted surface area

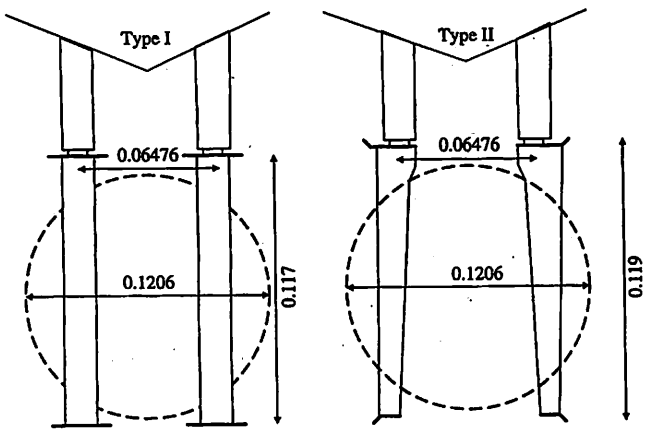

Fig. 3 View from the stern of twin-rudder system

Fig. 3. Each one of the twin rudders has the profile of the Schilling rudder and incorporates a rounded leading edge and a fishtail trailing edge. The twin rudder is also fitted with end plates on the top and bottom part of each rudder. In the twin rudder (type I), the cross-section of the port and starboard rudder is the same, the rudder cross-section does not have camber, the end plates are flat at the top and knuckled at the bottom and symmetrical about the centerline of each rudder. In a twin-rudder (type II) system, the cross-section of the port and starboard rudder is not symmetrical about its centerline, the rudder cross-section has a cambered profile and the end plates are knuckled and on the outboard side of each rudder.

Some important aspects may be noted here. Since the size of a single rudder is larger than a twin rudder, model ship A's stern is fabricated to accommodate both rudder systems. In case of a twin-rudder system, there is a gap between the skeg and aft transom that may reduce course stability of the vessel. When the twin rudder is fitted on the ship, the rudder is shifted towards the aft and the main hull is elongated by shifting the propeller aft within maximum existing ship length. This arrangement may improve course stability of the vessel and may increase the twin-rudder performance due to an increase in the lever of rudder moment. Due to the extension of the ship's hull, some increase in resistance is expected; however, propulsion efficiency may be further improved by fully optimizing the stern shape and the propeller for the twin-rudder system. The increased length of hull is expected to increase the cargo volume by about 1,000 m^3 for the subject ship type, without any change in the maximum ship dimension. In the case of a single rudder, there is a possibility that at ballast draft the rudder is near the free surface or even penetrates it; such an arrangement may cause air drawing or aeration. This possibility is reduced in a twin-rudder system. Due to its compact size, most of the twin-rudder system is in the way of propeller slipstream; therefore it is expected that it may utilize propeller slipstream more efficiently than a single-rudder system.

3.3 Experiment results

For a twin-rudder system, improvement in maneuvering performance has been shown in tail inboard operating conditions [7]. It was confirmed by free running experiments that this arrangement also improves propulsion performance (see Appendix). Therefore, during resistance and self-propulsion experiments, the twin-rudder system was set in 3° inboard angle position.

3.3.1 Rudder resistance experiments

Open water experiments were carried out in circulating water tank to determine rudder axial force characteristics. Only one of the twin rudders is used during experiments. In the case of type II and III twin-rudder systems, the port and starboard rudders are not symmetrical; starboard rudder is used for the experiments. Since, the resistance is measured for only one of the twin rudders; therefore, the total axial force of the twin rudder would be twice the value measured during the experiments.

The variation of axial force with inflow speed is investigated by varying the inflow speed, while the inflow angle is kept constant (0°). To induce turbulence, 3.0 mm wide sand paper strips were glued on both sides of the rudder at a

distance of 10% chord length from the leading edge of the rudder. The experiment results are shown in Fig. 4. For all types of twin rudders, the rudder axial force reduces with increase in Reynolds number and tends to a steady value for higher Reynolds number. The water inflow speed for all rudders is varied between 0.1 and 1.1 m/s. The Reynolds number is higher for the twin-rudder (type III, B) system, because of its larger size and higher water temperature during experiments. The results for twin-rudder (II) systems at low Reynolds number are influenced by partial laminar flow. This shows that flow-stimulating arrangement is not sufficient for this rudder type. However, the results at higher Reynolds number are more pertinent, because they well represent the actual flow speed in behind condition. The experiment results match well with the theoretical formulation described earlier.

The variation of axial force with inflow angle is investigated, by varying the rudder angle, while the inflow speed is kept constant (0.8 m/s). The Reynolds number is 5.96E + 04, 4.15E + 04 and 4.14E + 04 for single-rudder, twin-rudder (I) and twin-rudder (II) systems, respectively. A turbulence inducing device is not fitted on any one of these rudders. For a single rudder experiment, the rudder horn is installed, but only the force on the movable part of rudder is measured. This is because, in the actual layout, the rudder horn is part of the main hull. The experiment results are shown in Fig. 5. For the single rudder, the axial force marginally increases with increase of inflow angle, but the behavior is opposite for twin-rudders (type I, II) systems. For twin-rudders (type I, II) systems due to absence of turbulence inducing device, variation in axial force is not smooth near 0° inflow angle. The rudder cross-section for single-rudder and twin-rudder (I) systems is symmetrical, but there is some asymmetry in the experiment data. The regression curve for a single-rudder and a twin-rudder (I) system is determined by assuming it to be symmetrical.

The rudder axial force characteristics behind the ship, with and without the propeller, were also investigated. The case when the rudder is fitted behind the ship without a propeller will be called "without propeller", and the case when the rudder is fitted behind the ship with a propeller will be called "with propeller". No flow-stimulating device is fitted on any of the rudder systems during these experiments. The results are shown in Fig. 6. For both rudder systems, the experiments were carried out at similar model speeds and propeller revolutions. For a single rudder, the higher Reynolds number is due to its larger size and different geometric layout in comparison to the twin rudder. For a single rudder "without propeller", the axial force coefficient is lower than twin rudder and for higher Reynolds number even becomes negative. This may be due to the rudder horn and the stern hull form, which blocks the flow to the rudder, while some contributing factor may be the cross-section of the rudder. For the twin-rudder "without propeller", the axial force of a type II rudder is higher than that of a type I rudder. For a single rudder "with propeller", the axial force coefficient marginally increases in comparison to one "without propeller". For the twin rudder "with propeller", the axial force coefficient is much higher than one "without propeller". This difference in axial force coefficient between the two types of twin rudders reduces in the case "with propeller". For the twin rudder "with propeller", the axial force coefficient is higher than the value predicted by open water experiment (with turbulence inducing device). The increment of axial force for rudders with NACA type section when the rudder

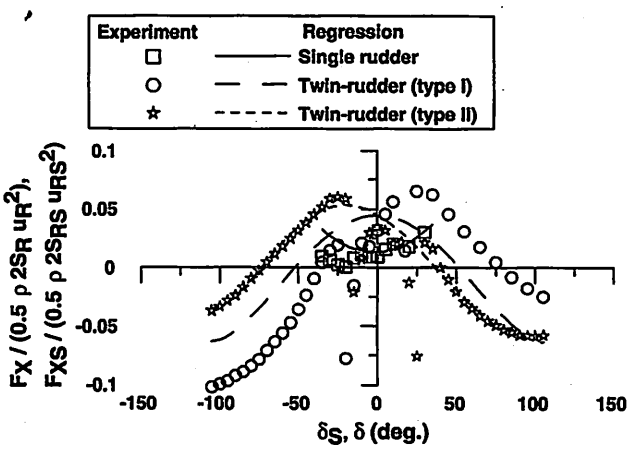

Fig. 5 Variation of rudder axial force with inflow angle observed during open water experiments

Fig. 4 Variation of rudder axial force with inflow speed observed during open water experiments

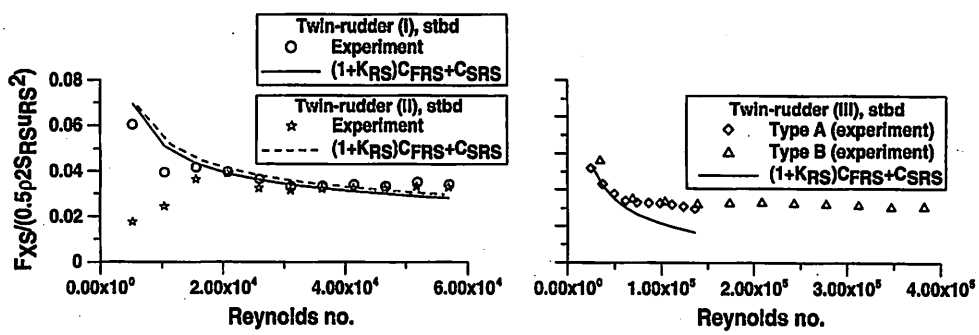

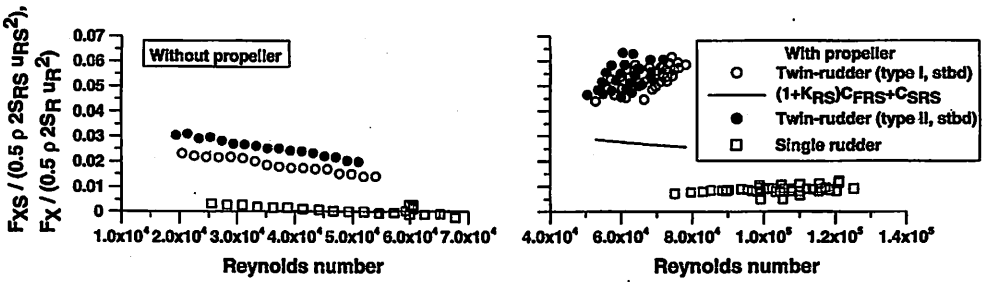

Fig. 6 Variation of rudder axial force with inflow speed. Rudder is installed on Model ship A

Table 3 Comparison of form factor of different twin rudders

Coefficient	Twin rudder				Holtrop et al. [18]		
	Experiment		Simulation [17] (Rn: 1×10^5)				
	Type I	Type II	Type I	Type II	Rudder behind stern	Twin-screw balance rudders	Rudder behind skeg
$1 + K_{RS}$	2.65	2.8	2.27	2.99	1.3–1.5	2.8	1.5–2.0
C_{SRS}	0.002	0.002					

For experiment analysis, rudder area = $2 \times S_{RS}$

is located at off-center position of the propeller in horizontal direction has been reported earlier [16].

It is concluded that axial force characteristics "without propeller" for all types of rudder has some influence of laminar flow, while the flow is turbulent "with propeller" for all types of rudder. For the twin rudder "with propeller", the axial force coefficient determined from the open water experiment (with turbulence inducing device) seems to be underestimated. The Reynolds number "with propeller" at model scale is in the range 5.28E + 04–7.82E + 04, while in the ship scale it is expected to be in the range 2.11E + 07–2.60E + 07. Therefore, variation of axial force coefficient for twin rudder with Reynolds number and rudder section needs to be investigated.

The influence of Reynolds number, the shape of the rudder section and the angle of attack on the axial force of different high lift rudders (including the one considered in this paper) was investigated by numerical simulation [17] and the variation of axial force with Reynolds number, shape of rudder section and angle of attack was shown. The twin-rudder section studied in this paper was also used for numerical simulation [17]. The values of $(1 + K_{RS})$ estimated from different sources are shown in Table 3. The coefficient C_{SRS} is considered to have a small constant value due to the fine shape of the rudder section. The form factor $(1 + K_{RS})$ estimated by numerical simulation [17] is higher for twin rudder (II) than for the twin rudder (I). The results of numerical simulation explains the experiment results observed in Fig. 6. In Fig. 4, some influence of laminar flow on the axial force of the twin rudder (II) is observed due to which its F'_{XS} is not higher than that of the twin rudder (I). The variation of axial force of twin rudder is significant [17] and the same is considered for analysis at full-scale.

3.3.2 *Propeller rudder interaction behind ship*

The wake characteristics in the way of the single-rudder and twin-rudder (type I) systems were determined from experiments. During the experiment, the rudder is fitted behind the ship, while the propeller is removed, and the shaft boss fitted with fair water cap. In the case of the twin rudder, only the starboard side rudder is fitted to avoid any interaction effects from the port side twin rudder. The model is towed at the same speed with different rudder angles. The rudder normal forces are measured during the experiment. By referring to the open water experiment results, average flow speed over the rudder is measured and the wake fraction in way of the rudder is calculated. The estimated value of the wake fraction is shown in Fig. 7. The values for twin rudder are higher than those for a single rudder; this is expected because of the difference in the layout of the two rudders. A comparison is also made with the values estimated for a different ship type and twin rudder [7]. For the straight line motion, average wake in the way of the rudder is considered as constant value based on experiment data. For full-scale analysis, the rudder wake is scaled up in the same ratio as the wake in way of the propeller.

Influence of propeller on rudder inflow characteristics were investigated by experiments. The propeller accelerates the flow speed to the rudder. The coefficient κ and $\kappa_{\{P\}}^{\{S\}}$ depends on the geometric layout of the propeller and

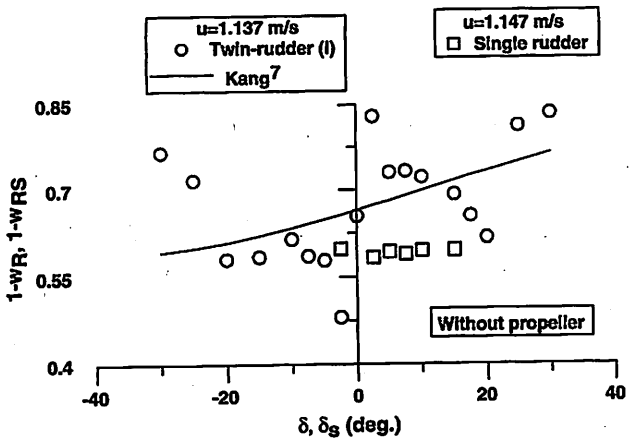

Fig. 7 Variation of average wake in way of single rudder and twin rudder. Rudder is installed on Model ship A

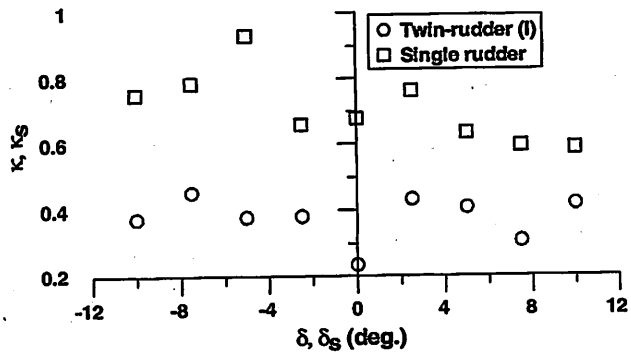

Fig. 8 Variation of κ and κ_s for different rudder systems. Model ship A

the type of rudder. Rudder lift forces for different propeller revolutions, ship speed and rudder angles were measured during the experiments in a towing tank. From the rudder lift force, rudder inflow velocity is estimated using open water experiment data. For the twin rudder, the rudder lift force is measured only for the starboard rudder. All the parameters in Eq. 3, except the coefficients κ and κ_S, are estimated from the experiment data. For the twin rudder, the experiments were conducted with both rudders, and their mutual interactions [7], were considered during analysis. The measured values of κ and κ_S are shown in Fig. 8. The coefficient κ is higher than the coefficient κ_S. This may be because, the single rudder is at the ship centerline and can fully utilize propeller slipstream, while the twin rudder is away from the ship centerline. However, each one of the twin rudders has a higher lift force coefficient, and the total effective area is higher than for the single rudder. These may compensate for lower κ_S.

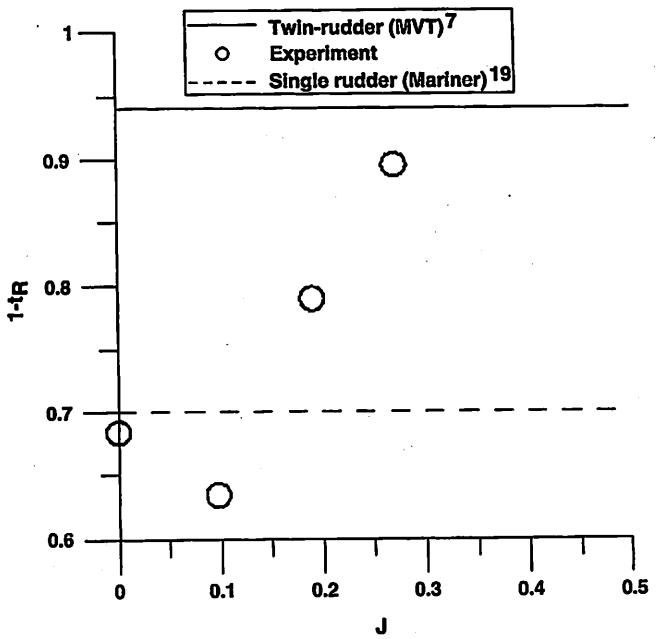

Fig. 9 Variation of t_R for the twin rudder (I) of model ship A. *MVT*, Mariner-type Vectwin rudder

3.3.3 *Hull rudder interaction coefficients*

Experiments were carried out to determine the coefficient $1 - t_R$. The values determined from experiment are shown in Fig. 9. The values of $1 - t_R$ for twin rudder (I) lie between single rudder [19] and other type of twin rudder [7]. The difference between the single rudder and twin rudder (I) is due to the difference in their geometric layout. The difference between the two types of twin rudder is due to the difference in their geometric layout and due to the modified approach of estimating rudder resistance that is followed in this paper.

3.3.4 *Hull propeller interactions*

Self-propulsion experiments were carried out to determine interaction coefficient between the hull and propeller for different rudder systems. To see the influence of axial force of each rudder system, the experiment was carried out with and without the rudder and the coefficients determined at ship self-propulsion point. The thrust deduction fraction calculated by the "conventional method" and "proposed method" is shown in Fig. 10. In the case of the single rudder, the thrust deduction coefficient determined by the "conventional method" and the "proposed method" is nearly the same. However in the case of the twin rudder, the "conventional method" gives a lower value of the coefficient than the "proposed method". For the twin rudder, the resistance experiments show that ship fitted with a twin rudder (type II) has a higher resistance than the

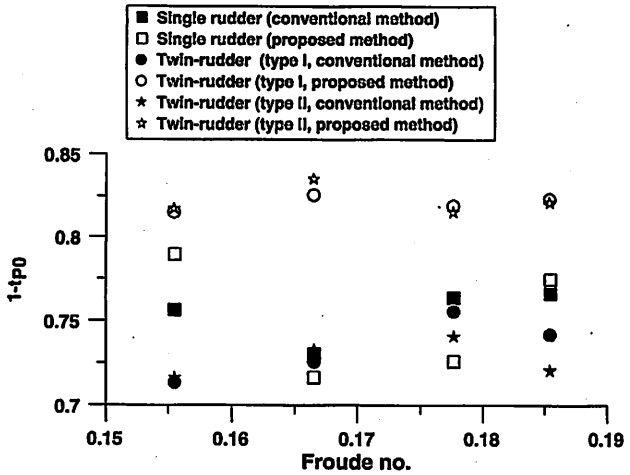

Fig. 10 Variation of t_{P0} for different rudder systems. Model ship A

ship fitted with a twin rudder (type I). However, the thrust deduction coefficient for both types of twin rudders is similar as per the "proposed method", while in the case of the "conventional method", the values of twin rudder (type I) are slightly higher. The reason for this is that the axial force characteristics of both types of twin rudder in "with propeller" conditions become nearly the same as shown in Sect. 3.3.1.

From the experiments, coefficients w_{P0} and η_R for the three rudder types were also estimated. The two analysis methods do not significantly change the values of these coefficients, so the values estimated by "proposed method" are shown in Fig. 11. The values of coefficient w_{P0} for the different rudder systems were observed to be similar. The values of coefficient η_R for the twin rudder are lower than for single rudder. This may be because, in the case of twin rudder, the rudders are offset from the centerline.

To investigate the influence of the twin rudder on coefficient ϕ in Eq. 9, experiments were carried out to estimate the coefficient w_{P0} both with and without the twin rudder. The experiment results are shown in Fig. 12. The difference in the value of w_{P0} with and without the rudder indicates the value of ϕ.

3.3.5 *Full-scale powering performance prediction*

The principal particulars of the Ship A and B are shown in Table 4. Ship A is used for investigating the difference in the power predicted by "conventional method" and "proposed method" for different rudder systems. Ship B is used for comparing the power predicted by the "conventional method" and the "proposed method" with the values measured during full-scale experiments for twin-rudder system.

For Ship A, power is predicted from model experiments by the "conventional method" and the "proposed method"

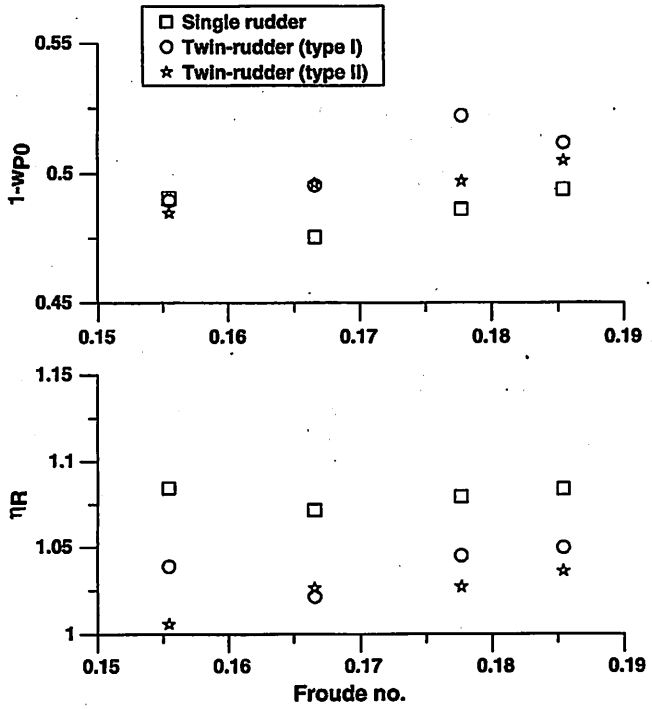

Fig. 11 Variation of w_{P0} and η_R for different rudder systems. Model ship A

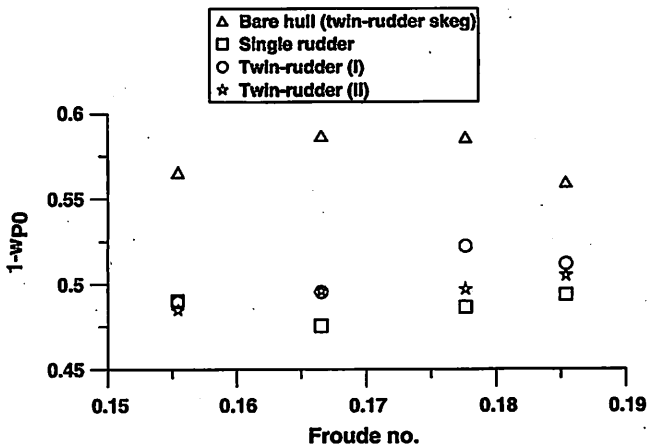

Fig. 12 Influence of different rudder types on wake fraction. Model ship A

by simulations. The steady state propeller revolutions and ship speed for constant torque operating condition of the engine were determined for four different speeds. Each one of the rudder system is considered to be installed with the same engine and shafting system. The shaft loss is considered to be 2% for both rudder systems. For all the rudders, propulsion efficiency improvement devices like propeller boss cap fin (PBCF) [20] and reaction fins were not considered. The engine power required to move the ship at a particular speed for each one of the rudder system is estimated by the "conventional method" and the "proposed method".

Table 4 Principal particulars of ship

Particulars	Ship A	Ship B
L (m)	219.00	99.20
B (m)	32.26	16.00
L_{OA} (m)	229.00	104.49
d_F (m)	13.30	5.54
d_A (m)	13.30	7.00
C_B	0.83	0.72
S_{BK} (m^2)	105.12	47.62
Propeller		
D_P (m)	6.70	3.40
P (m)	4.47	2.63
Number of blades	5.00	4.00
Projected area above waterline		
A_T (m^2)	655.50	96.00
A_L (m^2)	2,039.70	140.40

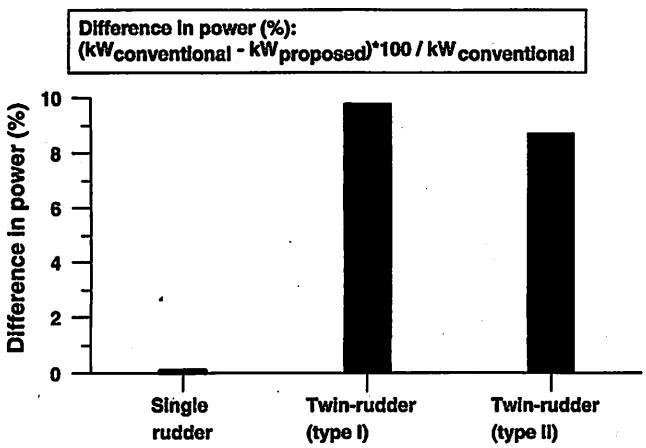

Fig. 13 Difference in the engine power estimated by "conventional method" and "proposed method" for different types of rudder. Mean values at Froude no. 0.175 for Ship A

The difference in the engine power estimated by the "conventional method" and the "proposed method" for each one of the rudder types is shown in Fig. 13. The difference in the engine power estimated by the "conventional method" and the "proposed method" is negligible for single rudder; however, it is significant for both types of twin rudder. The difference in engine power between the single rudder and twin rudder estimated by the "conventional method" and "proposed method" is shown in Fig. 14. The difference in engine power by the "proposed method" between single rudder and twin rudder (I) and single rudder and twin rudder (II), respectively, can be observed. There is no significant difference in engine power by the "conventional method" between the single

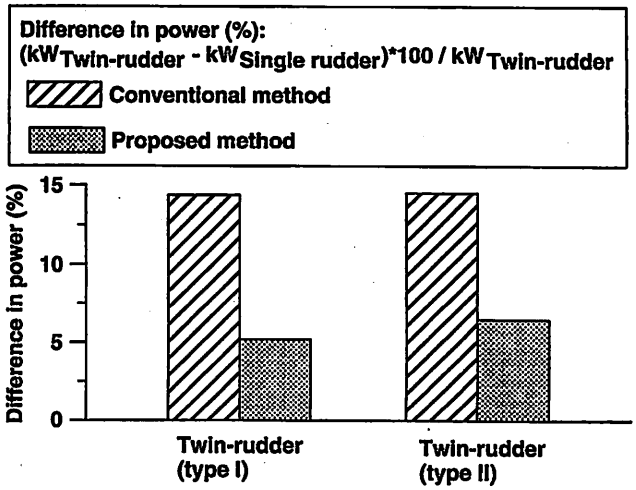

Fig. 14 Difference in engine power between single and twin rudder systems estimated by the "conventional method" and the "proposed method". Mean values at Froude no. 0.175 for Ship A

rudder and twin rudder (I) and single rudder and twin rudder (II), respectively. Therefore it can be concluded that the "proposed method" is sensitive to the influence of rudder axial force characteristics, while in the "conventional method", there is not much influence of rudder axial force characteristics. To confirm the suitability of either of the two prediction method, the predicted engine power by each method is compared with the values measured during full-scale experiments.

4 Full-scale experiments and discussion

To validate the results described in Sect. 3.3.5, the power predicted by the "conventional method" and the "proposed method" is compared with the values measured during full-scale experiments for model ship B. Experiments in towing tank were carried out with the model ship B (fitted with twin rudder type III) and full-scale power was predicted by the "conventional method" and "proposed method". Both predictions are for calm condition. The full-scale experiment was carried in the month of July. During the experiment, the ship's engine was operated at 50%, 75% and 100% of its maximum power. At each engine power setting, the ship was run on a straight course for a reasonable duration of time. Two runs were carried out for each engine power setting. During each run, the ship speed, engine power, propeller revolution, relative wind speed and relative wind direction were measured. These values are averaged for each run. No rudder angle is given during the experiment. The wave conditions during the experiment are obtained from the statistical database of wave and winds around Japan [21]. The wave direction is assumed to be the same as that of the wind. The wind and wave correction

was applied to the power measured during the experiment [22]. The ship was fitted with a PBCF on the propeller and horizontal reaction fins on the twin-rudder system, these were not fitted on the model ship. From model experiments, it is shown that about a 5% gain in efficiency may be obtained with a PBCF-type device [20]. Then it is expected that a 6–8% gain in propulsive efficiency may be obtained with a PBCF and reaction fins. In actual sea conditions, it is considered that the combined effect of these appendages is 4% on the ship's engine power. It should be noted that ship B has a bow thruster tunnel opening, which was not present in model ship B and no correction for bow thruster opening was applied. The power excluding PBCF, fin and weather influence is compared with the power predicted by the "conventional method" and "proposed method" from the model experiments. The results are shown in Fig. 15. The power (excluding weather influence, PBCF and reaction fin) matches well with the power predicted by the proposed method. The overestimation of engine power by the "conventional method" at higher speed due to uncorrected scaling of the rudder resistance can be observed.

From the experiment results and analysis, it is observed that the scale effects are present on the axial force of rudder, and it depends on the rudder cross-section and the Reynolds number. The rudder with the NACA section has a low axial force, so the scale effect on the axial force does not have much influence on the full-scale powering performance prediction. However, the influence of the scale effect on the axial force of special rudder systems like the Schilling rudder and twin rudder may be significant. The influence starts from the model ship resistance experiments. During resistance experiments, the flow at the aft part of the ship is usually reduced by the ship's geometry and the flow acceleration effect of the propeller is absent, so the average flow over rudder is low. This condition is more severe for compact rudder systems like Schilling, twin rudder etc., because they have a special section and lower chord. For the same model speed, they operate at lower Reynolds number than the single rudder; therefore their axial force component is comparatively higher. Therefore, the model ship installed with special rudder systems like the twin rudder has a comparatively higher resistance than the model ship installed with a single rudder. This difference in resistance is not the same during the model self-propulsion condition and at the full-scale condition. The higher model ship resistance is transformed into an increased form factor and residuary wave-making resistance, respectively. The increased form factor is multiplied by the total ship area and ship speed, though there is a compensatory effect of reduced frictional resistance coefficient. The residuary wave-making component is multiplied by the total ship area as well as the ship speed. The combined effect of these two may result in the overestimation of power by the "conventional method" in the case of ship fitted with special rudder systems like twin rudder system. It would be interesting to make similar comparison for other ship types.

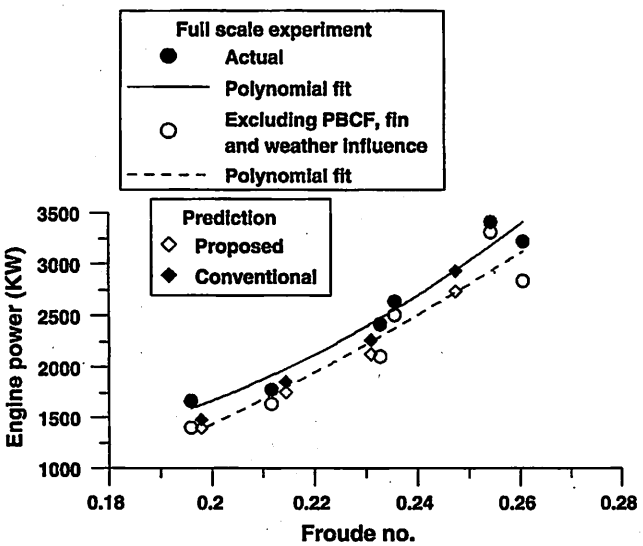

Fig. 15 Comparison of power predicted from model experiments with the full-scale values. Ship B (fitted with a twin rudder, type III)

5 Conclusions

In this paper, single rudder and twin rudder systems have been compared from the aspect of propulsion performance. The following are the conclusions of the paper:

1. The scale effect is present on the axial force of both single and twin rudders. In the case of a ship fitted with a single rudder, because of the low axial force, the power predicted by either considering or ignoring this scale effect is nearly the same. However, in the case of a ship fitted with a twin rudder, the power predicted by ignoring this scale effect may be about 8–9% (depending on the twin rudder cross-section) higher than the case when the scale effect is considered.
2. A new method, the "proposed method", of determining full-scale power of ships is developed, where the rudder axial force and the model ship resistance are considered separately. It is shown by model and full-scale experiments that the power predicted by the "proposed method" is also suitable for ships fitted with twin rudder system.
3. For the "proposed method", the MMG-type model is used for determining rudder inflow velocity. It is

shown that the coefficients of MMG-type model for rudder inflow velocity are different for single and twin rudders.

Acknowledgments The authors gratefully acknowledge advice of Prof. Y. Toda, Osaka University and Dr. H. Tatano, Japan Hamworthy Co. Ltd, during the course of experiments and analysis. The authors also thank Mr. Y. Gonno and Mr. Y. Uematsu, master course students, Department of Ocean Engineering and Naval Architecture, Osaka University, for their help during the experiments.

Appendix

1 Influence of tail inboard angle of twin-rudder

Free running experiments were carried out with model ship B to see the influence of tail inboard angle of twin-rudder system on ship speed. Before each run, the twin-rudder is physically set to the respective inboard angle condition. During the experiment, the model is run on a straight course using autopilot. The experiment is done in good weather condition, so the average respective rudder angle during the experiment is equal to the set inboard angle. All the experiments were carried out with constant propeller revolution. The average speed measured during the free running experiments at different settings of tail inboard angle is shown in Fig. 16. It is observed that maximum speed is achieved between the angle 2 and 4°.

2 Ship resistance experiments

The ship resistance experiment result is shown in Fig. 17.

3 Propeller open water characteristics

The full-scale propeller thrust and torque characteristics are shown in Fig. 18. During model experiments, the same stock propeller is used for model ship A and B. For ship A, the full-scale characteristics were determined by applying scale effects to propeller open water experiment results as per "conventional method". For ship B, the characteristics of design propeller were provided by the shipyard.

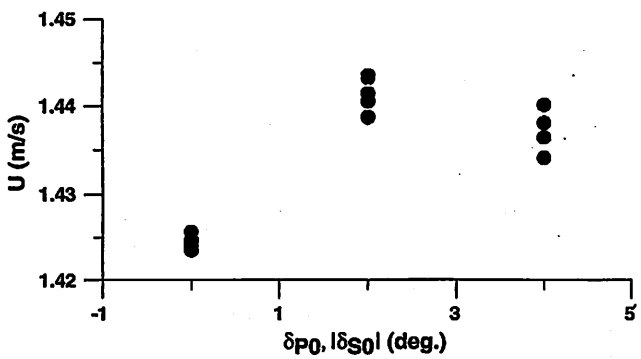

Fig. 16 Influence of inboard angle setting of twin rudder on ship speed for model ship B. $\delta_{\{S\}_0}$, tail inboard angle for a twin rudder [7]

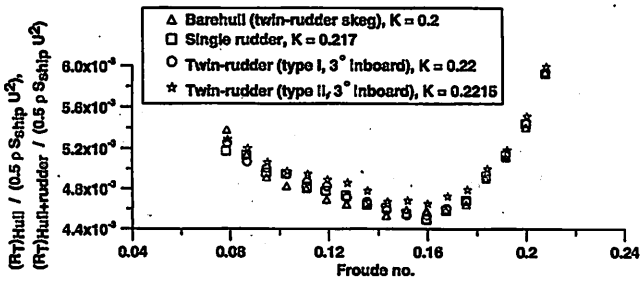

Fig. 17 Comparison of resistance of model ship A fitted with different rudder systems. For a bare hull $S_{ship} = S_W$, for hull with a single rudder $S_{ship} = S_W + 2.0S_R$, for a hull with a twin rudder $S_{ship} = S_W + 2.0(S_{RS} + S_{RP})$

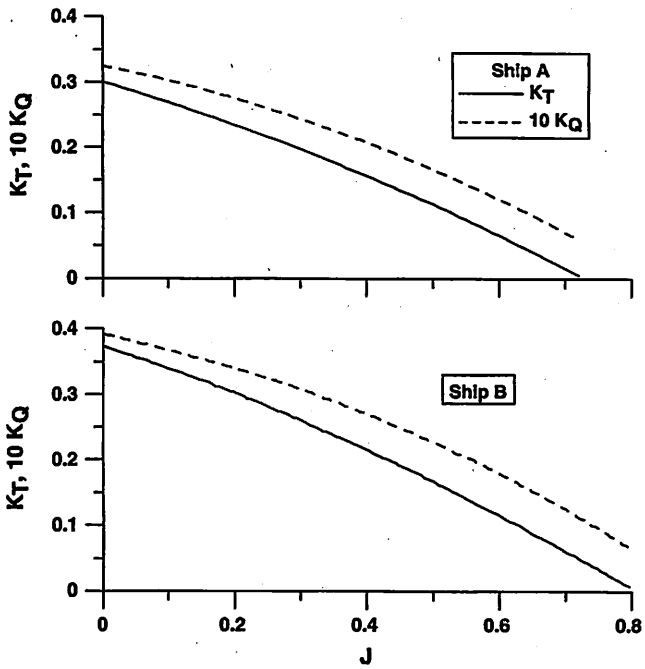

Fig. 18 Propeller open water characteristics

References

1. Yamada K (2003) Application of ship-handling/manoeuvrability criteria to stern configuration and rudder area design, Proceedings of MARSIM'03, Kanazawa, Japan, pp RB-4-1-RB-4-10
2. Lewis EV (1989) Principles of naval architecture. SNAME III:365
3. The Naval Architect (1985) The Royal Institution of Naval Architects, p E185

4. Japan Hamworthy & Co. Ltd, http://www.japanham.co.jp
5. Weinig F (1947) Lift and drag of wings with small span, NACA TM 1151
6. Hasegawa K, Kang DH, Sano M et al (2006) Study on maneuverability of a large vessel installed with a mariner type super vectwin rudder. J Mar Sci Technol 11:88–99
7. Kang DH, Nagarajan V, Hasegawa K et al (2008) Mathematical model of single-propeller twin-rudder ship. J Mar Sci Technol 13:207–222
8. Proceedings of 15th International Towing Tank Conference (1978) The Hague, Netherlands
9. Proceedings of 24th International Towing Tank Conference (2005) vol II, Edinburgh, UK
10. Todd F H (1946) The fundamentals of ship propulsion. Transactions of the Institute of Marine Engineers, vol 58, London
11. Lewis EV (1988) Principles of Naval Architecture. SNAME II:14
12. Whicker LF, Fehlner LF (1958) Free stream characteristics of a family of low aspect ratio control surfaces for application to ship design, DTRC report 933
13. Shiba H (1960) Model experiments about the maneuverability of turning of ships, First symposium on ship maneuverability, DTRC report 1461
14. MMG (1980) MMG report V. Bull Soc Nav Archit Jpn 616:565–576 (in Japanese)
15. Kobayashi E, Kagemoto H, Furukawa Y (1995) Mathematical models of maneuvering motions. In: Research on ship maneuverability and its application to ship design. Proceedings of the 12th marine dynamic symposium, pp 23–89 (in Japanese)
16. Nakatake K, Ando J, Kataoka K et al (1989) Study on the propulsive performance of twin screw ship—interaction between propeller and rudder in a uniform flow. Trans West-Jpn Soc Nav Archit 78:49–57 (in Japanese)
17. Murakami A, Kawamura T, Arii T (2007) Evaluation of the scale effects of high lift rudders by numerical simulation. In: conference proceedings of The Japan Society of Naval Architects and Ocean Engineers. vol 4, JASNOE, pp 305–308 (in Japanese)
18. Holtrop J, Mennen GGJ (1982) An approximate power prediction method. Int Shipbuild Prog 29:166–170
19. Hasegawa K (1980) On a performance criterion for autopilot navigation. J Kansai Soc Nav Archit 178:93–104
20. Gearhart WS, McBride MW (1989) Performance assessment of PBCF type device. In: Proceedings of 22nd American Towing Tank Conference
21. National Maritime Research Institute, http://www.nmri.go.jp
22. Fujiwara T, Ueno M, Ikeda Y (2006) Cruising performance of a large passenger ship in heavy sea, Proceedings of the 16th International Offshore and Polar Engineering Conference, San Francisco, California, pp 304–311